Soil Dynamics and Earthquake Engineering 164 (2023) 107637

Contents lists available at ScienceDirect

Soil Dynamics and Earthquake Engineering

journal homepage: www.elsevier.com/locate/soildyn

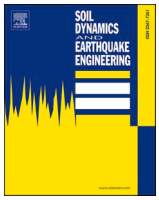

Analytical fragility curves for abandoned tailings dams in North-Central Chile

Gonzalo Boada [a], Cesar Pasten [b,*], Pablo Heresi [c]

[a] Department of Civil Engineering, University of Chile and Geotechnical and Tailings Area, SRK Consulting, Chile
[b] Department of Civil Engineering and Advanced Mining Technology Center (AMTC), University of Chile, Santiago, Chile
[c] Departamento de Obras Civiles, Universidad Técnica Federico Santa María, Chile

ARTICLE INFO

Keywords:
Fragility curves
Slope stability
Abandoned tailings dams
Performance-based earthquake engineering
Seismic displacements
Finite elements

ABSTRACT

Chile has 173 abandoned tailings dams with unknown seismic vulnerability levels due to uncertainties in their design, construction, operation, and closure stages. The physical stability of these geo-structures concerns the local communities and authorities in areas with high seismic hazard, given their deficient performance during past mega-earthquakes. This work develops fragility curves to estimate the expected damage as a function of the spectral acceleration Sa(0.3 s), based on dynamic analyses of a representative 2D FEM model, subjected to ground motion records of interface earthquakes, following a Multi-Stripes Analysis. The proposed fragility curves provide the probability of attaining three damage levels for different yield seismic coefficients. Results indicate that abandoned tailings dams in Chile have significant probabilities of severe earthquake-induced damage for Sa (0.3 s) > 1 g.

1. Introduction

The 2010 Mw 8.8 Maule, Chile Earthquake caused severe damage to five tailings dams [1], four of which were abandoned [2], increasing the interest of the mining industry, the authorities, and the society on the failure risk of these abandoned geotechnical structures. Abandoned tailings dams are geotechnical structures designed and operated more than twenty years ago by small- and medium-size copper and gold mining companies that currently lack an identifiable responsible owner. For this reason, the National Geology and Mining Service (Sernageomin) is currently responsible for the oversight of these structures with a limited budget, compared to that required for an exhaustive evaluation of their physical stability. Chile is the third country with most tailings dams, behind China and the United States. From the 757 tailings dams in Chile, 15% are active, 62% inactive, and 23% abandoned [3]. Therefore, the physical stability evaluation of the 173 abandoned tailings dams is difficult due to inherent regulatory difficulties, budget limitations, and lack of information regarding their design, construction, operation, and closure stages [4].

Several abandoned tailings dams are near to populated areas, waterways, roads, and productive activities, causing financial and administrative problems for the territorial authorities, the discontent of the neighboring communities, risk of contamination, and concerns associated with the physical instability of these structures. In this context, the seismic hazard has a fundamental role in the physical instability, considering that 82% of the 38 historical failures of tailings dams reported in Chile have been triggered by earthquakes [2].

Evaluating the seismic stability of abandoned tailings dams is a complex task due to the uncertainty in the seismic process, in the materials that compose the structure, and in the decisions adopted during their design and construction stages. A proper analysis requires a detailed characterization of the stored tailings, the dam materials, and the foundation soil, which is costly considering the number of abandoned tailings dams. For this reason, this study develops a tool that can help the estimation of the seismic physical stability and a first-order estimate of the seismic risk of these geo-structures while site-specific data is obtained by the authorities. The results can inform decisions of investment in further geotechnical characterization or reinforcement of the most vulnerable dams that can threaten the neighboring communities and ecosystems.

Performance-Based Earthquake Engineering (PBEE) provides a probabilistic framework that helps to improve the stakeholders' seismic-risk decision-making based on objective and scientifically rigorous methodologies [5]. One of the elements of the PBEE framework is the

* Corresponding author. Av. Blanco Encalada 2002, Of. 431, Santiago, 8370449, Chile.
E-mail address: cpasten@uchile.cl (C. Pasten).

https://doi.org/10.1016/j.soildyn.2022.107637
Received 9 September 2022; Received in revised form 30 October 2022; Accepted 30 October 2022
Available online 12 November 2022

fragility curve that allows estimating the probability of attaining different damage states in a structure conditioned on a seismic intensity measure.

Few fragility curves have been developed for geotechnical structures compared to those created for structural engineering applications. Some curves have been developed mainly for components of road systems such as cuts, embankments, and cantilever retaining walls [6–8]. These curves are not applicable for estimating the stability of abandoned tailings dams in Chile because: (1) these curves have been mainly calibrated with seismic records of shallow-crustal earthquakes, which have different characteristics compared to the megathrust earthquakes produced in the Chilean subduction zone; and (2) the proposed damage states are based on serviceability aspects. In contrast, abandoned tailings dams do not present relevant levels of serviceability.

This study seeks to generate a methodology for developing analytical fragility curves for abandoned tailings dams in North-Central Chile through the analysis of nonlinear 2D numerical models subjected to sets of scaled Chilean seismic records. The study evaluates the efficiency of different seismic intensity measures and proposes a probabilistic relationship between damage states and the seismic response, given by the residual stress state of a representative numerical model.

2. Characterization of abandoned tailings dams

In Chile, an abandoned tailings dam can store from 100 m^3 up to 600,000 m^3 of tailings materials. These structures total 173 in the country and 136 are primarily distributed within the North-Central region, between the parallels 28°S and 34°S. The potential collapse of one of these structures could affect the population, environmental systems, economic activities, and roads [3]. Fig. 1 shows a map with the location of the abandoned tailings dams in the study area.

North-Central Chile is a highly active seismic area, given the subduction margin between the Nazca and South American tectonic plates. Historically, the zone has been affected by megathrust interface earthquakes, such as the 1730 Central Chile Earthquake, with an estimated magnitude over Mw 9.0, the earthquakes in the Illapel zone in 1880, 1943, and 2015, and the 1971 Mw 7.8 La Ligua Earthquake. The area has been also hit by intermediate-depth intraplate earthquakes, such as the 1997 Mw 7.1 Punitaqui Earthquake. Estimates of the rupture length of megathrust interface earthquakes and the epicenter of the 1997

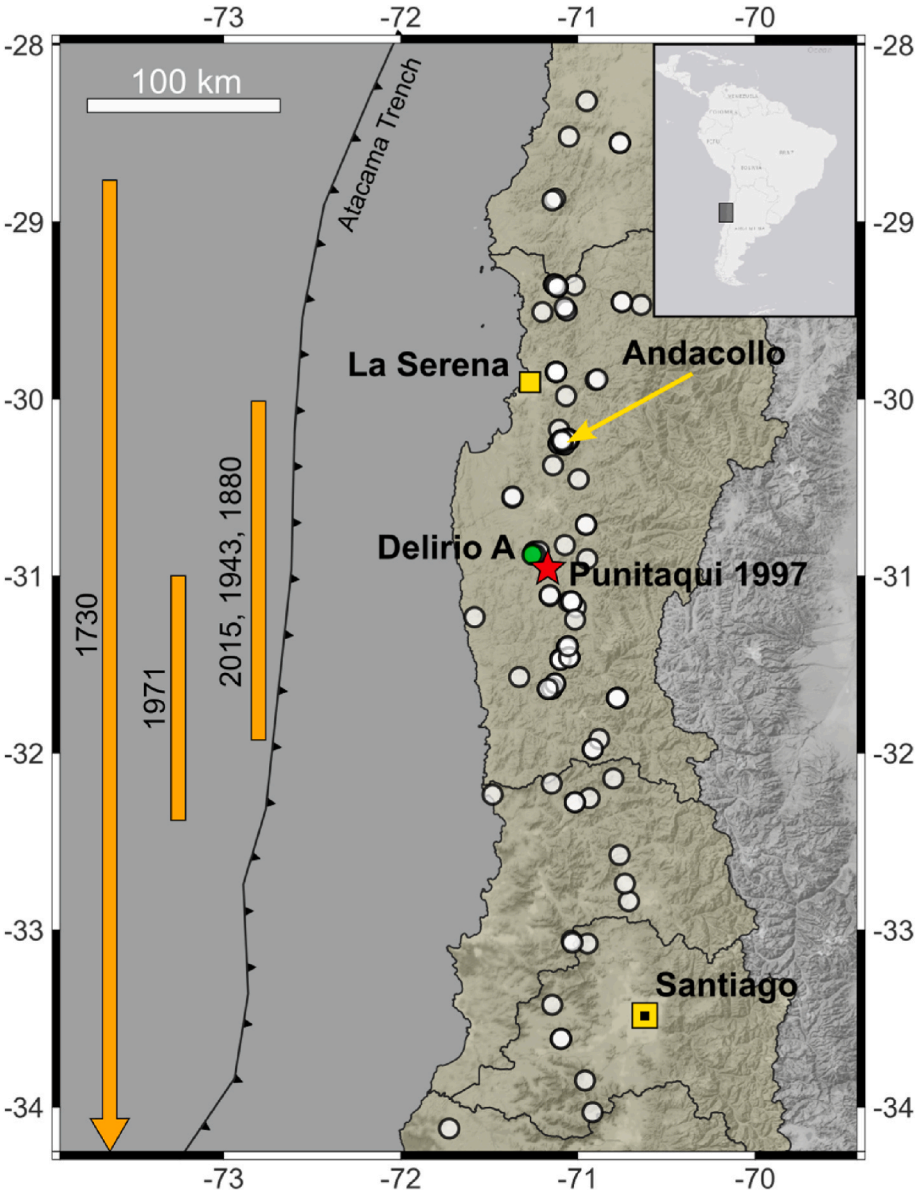

Fig. 1. Location of the 136 abandoned tailings dams in North-Central Chile.

Punitaqui Earthquake are shown in Fig. 1 [9,10].

An exploration campaign was carried out in the study area to characterize these abandoned tailings dams [11], which allowed us to estimate the parameters that control the dynamic behavior of our numerical models. In general, the materials of the dams do not differ from the stored tailings. The materials are mostly dry or with low water contents due to the long-term loss of water favored by the arid weather where these dams are located. The dam slopes are usually around H:V = 2:1, and they are founded over stiff soils or directly on rock outcrops.

One of the surveyed structures is the Delirio A tailings dam (Fig. 2a), with a height of approximately 21 m, adjacent to the Delirio B tailings dam. The Delirio B dam is composed of sandier materials than those of the Delirio A, and shows a collapse on its northwest slope, presumably caused by flow failure during the 1997 Punitaqui Earthquake. Fig. 2a shows a satellite image of both structures.

We performed a geophysical characterization of 6 abandoned tailings dams in the Coquimbo Region in order to obtain representative shear wave velocity profiles of the tailings materials and their structural predominant vibration frequencies. In the Delirio A dam, Tromino seismographs were installed, according to Fig. 2a, to record two 40-min sets of seismic ambient noise.

Fig. 2b shows the spectral amplifications obtained from two procedures: (1) the Horizontal-to-Vertical Spectral Ratio method (HVSR [12]), and (2) the Standard Spectral Ratio method (SSR, [13]). For the first method, four seismographs were placed over the tailings dam. The spectral ratios between the horizontal and vertical Fourier spectra were calculated considering 25-s windows. The HVSR curve shown in Fig. 2b is the geometric average of the 80-min records in each of the 4 seismographs. For the calculation of the SSR, two seismographs were located over the structure and two over the foundation soil at the dam toe. The ratios between the smoothed Fourier spectra of the horizontal components recoded over the dam and at the dam toe were computed, also considering 25-s windows. The SSR curve shown in Fig. 2b is the geometric mean of all possible combinations between sensors' components. The signal processing was performed with the Geopsy software [14]. We identified that Delirio A presents a predominant vibration frequency of 3 Hz. The similarity of the results obtained with both methods suggests the high stiffness of the foundation soil in the studied tailings dam.

Fig. 2c shows the estimated shear wave velocity profile of the Delirio A dam, obtained using the cross-correlation method described in Ref. [15]. The tailings material can be associated to a nearly constant shear wave velocity of 250 m/s. There is also a high-velocity contrast at the interface between the tailings and the stiff foundation soil at a depth similar to the dam height (i.e., 21 m).

The mean shear wave velocity of the six surveyed abandoned tailings

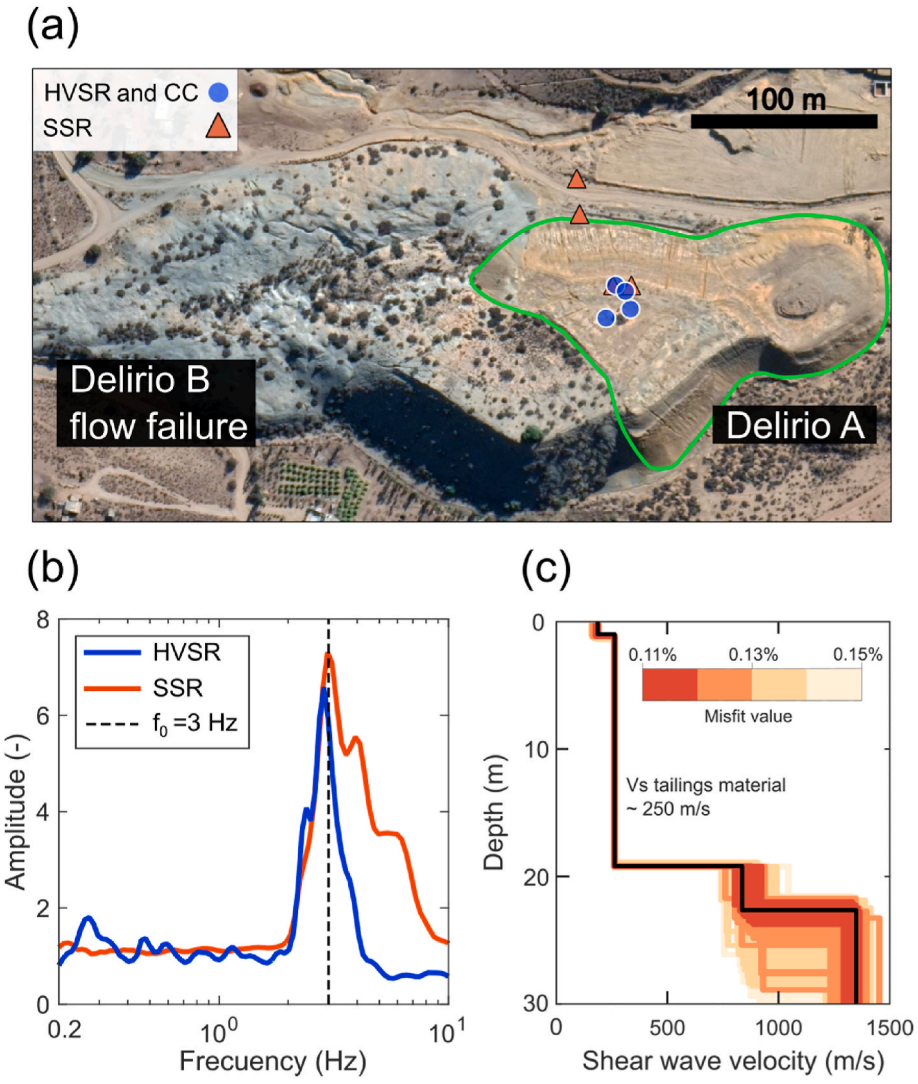

Fig. 2. (a) Satellite image of the Delirio A and Delirio B abandoned tailings dams and the position of the Tromino seismographs for measurements of seismic ambient noise. (b) Estimates of predominant vibration period from the HVSR and SSR methods. (c) Representative shear wave velocity profile of the Delirio A tailings dam.

dams is 205 m/s, with a standard deviation of 31 m/s. On the other hand, the predominant vibration frequency f_0 was found to be consistent with the value predicted by the one-dimensional wave propagation theory, $f_0 = Vs/(4H)$, where Vs is the average shear wave velocity and H is the tailings dam height.

The tailings stored in these abandoned deposits are mainly sands with variable fine content. The shear strength parameters of the tailings, cohesion (c′) and friction angle (φ′), were inferred from results of laboratory simple shear tests performed on tailings materials on dry conditions from the Delirio A and Delirio B tailings materials [11]. We adopted an internal friction angle φ = 30° and cohesion c = 7 kPa. As the cohesion has a high intrinsic variability [16], additional analyses considering different cohesion values were performed and presented in Section 5. Field estimates show that the slope angles of these structures vary between 28° and 35°, which are mainly defined by the upstream deposition method [17]. In this study, we adopted a constant representative slope angle of 30°.

According to the analysis of 70 abandoned tailings dams in the study area [11], 45 dams are smaller than 10 m height, 22 dams are between 10 and 20 m height, and only 3 dams are larger than 20 m height. Considering these heights, we assumed that 15 m is a representative height of a tailings dam whose physical instability could cause severe consequences to the neighboring communities and ecosystems. Note that these dams are considerably smaller than active tailings dams of large-scale mines that can reach hundreds of meters height.

3. Numerical model

The information summarized in the previous section was used to define a representative 2D numerical model of the abandoned tailings dams in North-Central Chile. The model was implemented in the Plaxis2D finite-element method (FEM) software [18].

The model is a homogeneous, 15 m high slope with an inclination angle of 30°, discretized into 15-nodes plane-strain finite elements with 12 integration points. The slope consists of tailings material founded on an elastic 30 m depth layer with a shear wave velocity of 800 m/s (Fig. 3).

A water table was not considered inside the slope since the materials are mostly dry or with low water contents due to the long-term loss of water favored by the arid weather in North-Central Chile.

The input motion at the model base is obtained from a deconvolution process using the DeepSoil v7 software [19] in order to obtain the target ground-motion record at the Free Field control point (see Fig. 3). The lower boundary condition is “None” and considers a kinematic input, corresponding to an acceleration time-history record, through the “Prescribed displacement” condition. The lateral boundaries of the model are "Free Field," which prevents reflection of seismic waves while preserving the input motion at the base [18]. Different control nodes are defined inside the model domain in order to follow the kinematic response of the interest zones (C1, C2, C3, and C4 in Fig. 3).

The foundation of the model is assumed linear-elastic with parameters shown in Table 1. The assigned properties are consistent with the high impedance contrast between the tailings and the foundation soil, evidenced during the geophysical field campaign. Additionally, a Rayleigh damping fraction is included according to considerations in Ref. [20].

Table 1
Properties of the linear elastic model defined for the foundation soil.

Property	Units	Value
Specific weight, γ	kN/m^3	20
Young's modulus, E'	MPa	3392
Poisson's ratio, ν'	-	0.3
Shear wave velocity, V_s	m/s	800
α of Rayleigh Damping	–	1.38
β of Rayleigh Damping	–	$6.43 \bullet 10^{-4}$

The tailings mechanical behavior is captured with the Hardening Soil with Small Strain (HSS) constitutive model (Schanz et al., 1999), defined as an isotropic hardening model with stiffness degradation at small strains that describes the hysteretic behavior of soils. Since the model shear modulus is a function of the effective confinement, the model can capture the increase in shear wave velocity with depth. Table 2 shows the values adopted for the HSS model parameters. The shear wave velocity of the model ranges from 125 m/s at the slope crown to 245 m/s at the slope base, which is slightly conservative compared to the shear wave velocity profile shown in Fig. 2, but compatible with the average Vs = 205 m/s calculated from various abandoned dams.

The stiffness degradation and damping curves predicted by the HSS constitutive model are equivalent to the curves proposed by Ref. [21] for granular materials with low-medium plasticity, as shown in Fig. 4. Fig. 4 also shows the range of stiffness degradation proposed by Ref. [22], used to represent the behavior of copper tailings and slimes. A small Rayleigh damping fraction is included to capture non-hysteretic energy dissipation mainly at very small strains.

Table 2
Properties of the Hardening Soil with Small Strain (HSS) model defined for the tailings material.

Property	Units	Value
Dry specific weight, γ	kN/m^3	17
Reference deviatoric deformation modulus, E_{50}^{ref}	MPa	6
Reference oedometric modulus, E_{oed}^{ref}	MPa	4
Reference discharge and reload modulus, E_{ur}^{ref}	MPa	36
Power parameter, m	–	0.5
Cohesion, c'	kPa	7
Friction angle, φ'	°	30
Dilatancy angle, ψ'	°	0
Elastic Poisson ratio, ν_{ur}	–	0.2
Stress ratio, R_f	–	0.9
Reference stress, p_{ref}	kPa	100
Reference shear modulus, G_0^{ref}	MPa	80
Reference value of shear strain, $\gamma_{0.7}$	–	$3 \bullet 10^{-4}$
α of Rayleigh Damping	–	0.3456
β of Rayleigh Damping	–	$1.607 \bullet 10^{-4}$

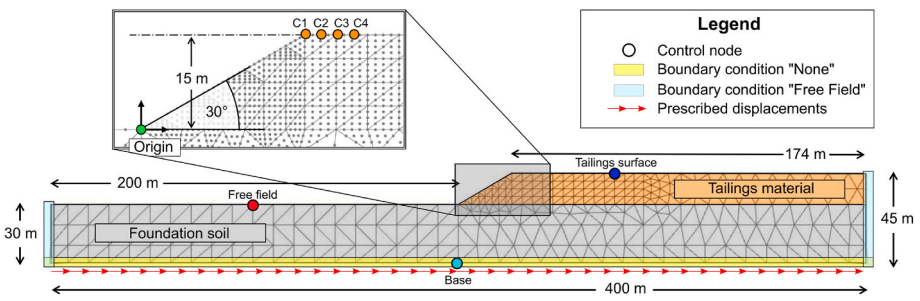

Fig. 3. Numerical model of abandoned tailings dams in the North-Central Chile.

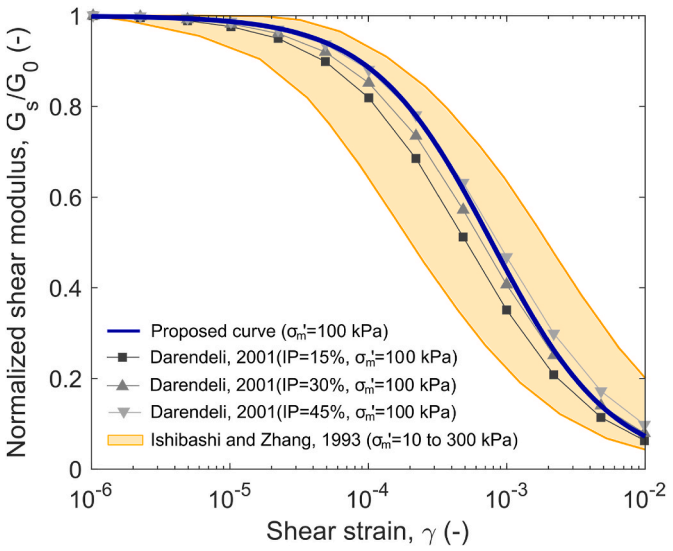

Fig. 4. Proposed stiffness degradation curve compared with curves obtained by Refs. [21,22].

The material properties and the mesh size allow proper simulation of wave propagation up to 40 Hz in the foundation layer and 20 Hz in the tailings, according to the criterion by Kuhlemeyer and Lysmer [23].

The numerical model accumulates shear strains when subjected to a dynamic seismic loading. Residual deformations are then referred to as permanent seismic displacements, commonly used to evaluate the seismic performance of earth slopes [24]. Fig. 5 shows the evolution of the vertical displacements of nodes C1, C2, C3, and C4, as a ground motion is applied at the base. The target ground motion considered in this example was recorded by the Chilean National Seismological Center (CSN) at the station PB06 (−22.7, −69.6) in the EW direction during the 2007 Mw 7.7 Tocopilla Earthquake. The record was scaled by a factor of 3.0. In Fig. 5, the vertical displacement increases with the largest velocity pulses of the ground motion. Fig. 6 shows the final state of the slope in terms of permanent displacements in the vertical and horizontal directions. These contours are complemented with the critical surface obtained from a pseudo-static limit equilibrium analysis performed in the GeoStudio SLOPE/W software [25], using the Morgenstern-Price method [26] for a horizontal seismic coefficient $k_h = 0.201$.

In the PBEE framework, the seismic response is condensed into Engineering Demand Parameters (EDP). We selected the average between the permanent vertical displacements of control nodes C1 and C2, *Uy*, as the EDP of the tailings dam. This choice is consistent with the fact that the vertical settlement of the crest is commonly related to damage in dams [27,28] and that the critical pseudo-static failure surface mainly compromises the displacement of nodes C1 and C2 (Fig. 6). Therefore, *Uy* can represent the permanent vertical displacement of the critical failure wedge. As shown in a later section of the present article, the plastified zone also starts developing between nodes C1 and C2, consistently with the critical surface obtained through pseudo-static limit equilibrium analysis.

4. Preliminary stage and selection of ground motions

Fragility curves define the probability of structural damage conditioned on a ground-motion parameter, known as Intensity Measure (IM). For selecting an optimal IM, three characteristics are usually evaluated: efficiency, sufficiency, and predictability. Efficiency is related to the certainty with which IM estimates the EDP [29]; sufficiency refers to the independence between the adopted IM and other ground motion parameters [30]; and predictability refers to the uncertainty in predicting the IM at the site of interest [31].

In this work, the focus is on studying the efficiency of different IMs to estimate the seismic displacements in the numerical model. For this purpose, we performed a Cloud Analysis to assess the correlation between different IMs and *Uy* in the slope model subjected to 169 instrumental seismic records of interface earthquakes with moment magnitudes larger than Mw 7.7 recorded in the Chilean territory: the 1985 Mw 8.0 Valparaiso, the 2007 Mw 7.7 Tocopilla, the 2010 Mw 8.8 Maule, the 2014 Mw 8.2 Iquique, and the 2015 Mw 8.3 Illapel Earthquakes [9].

Only high-magnitude earthquakes are tested due to the combined effect of the frequent occurrence of high-magnitude interface earthquakes in the study area [32] and the importance of the ground motion duration on the accumulation of seismic slope displacements, for which the magnitude is a proxy [33]. In fact, several simplified models that estimate seismic slope displacements consider the earthquake magnitude to capture the effect of duration [24,33,34].

We obtained the slope displacements as a function of ten IMs calculated in the free field of the model (see control point in Fig. 3) for the 169 dynamic model simulations. Fig. 7 shows examples of the

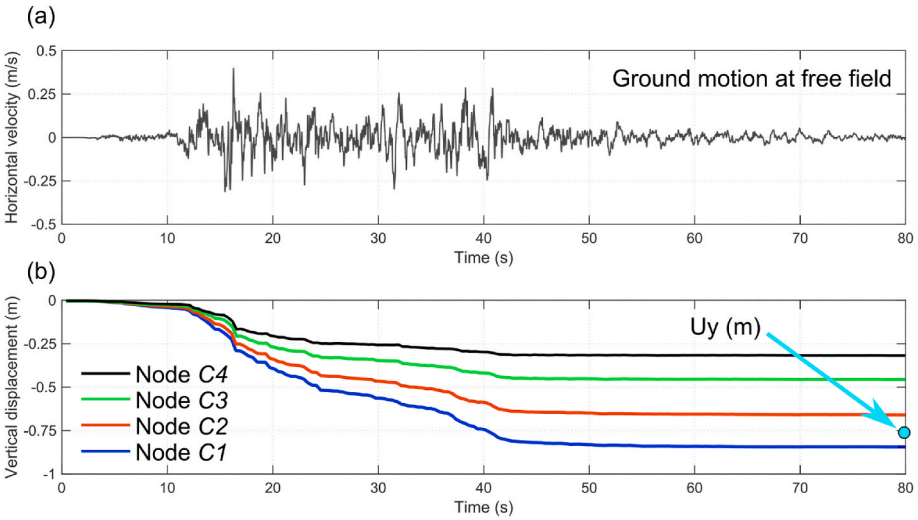

Fig. 5. Seismic response of the tailings dam model when subjected to the ground motion recorded in the EW direction at station PB06 during the 2007 Tocopilla Earthquake, scaled by a factor of 3.0. (a) Ground motion velocity time-history recovered at Free Field control point (Fig. 2). (b) Evolution of the vertical displacement at control nodes C1, C2, C3 and C4 (Fig. 3). *Uy* is the mean of the vertical permanent displacements in C1 and C2.

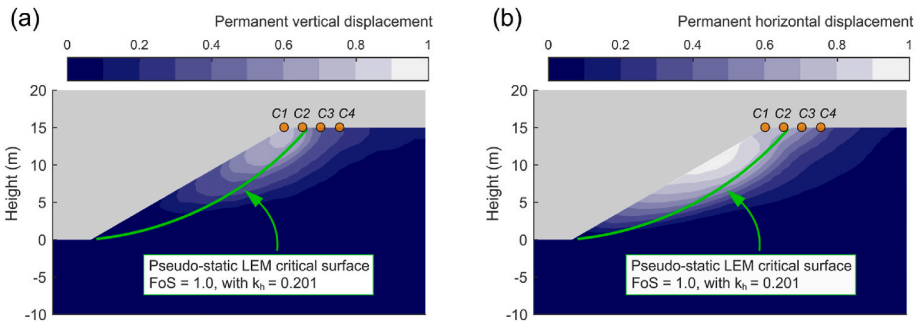

Fig. 6. Contours of permanent (a) horizontal, and (b) vertical nodal displacements. The crest control points (C1, C2, C3, and C4) and the critical surface from a pseudo-static limit equilibrium method (LEM) analysis with a horizontal seismic coefficient $k_h = 0.201$ are also shown.

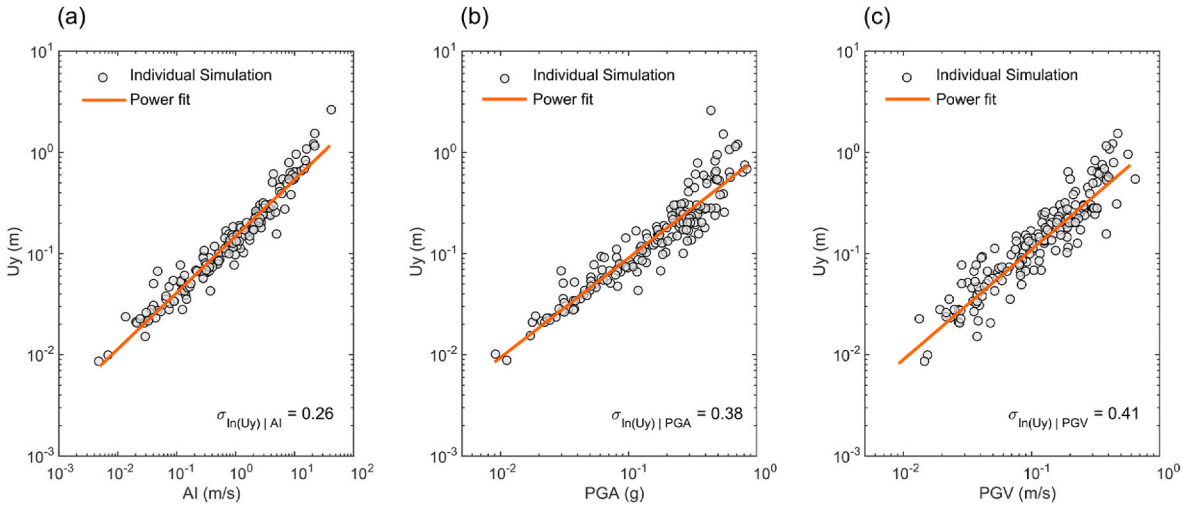

Fig. 7. Correlation between the permanent vertical displacement (*Uy*) of the abandoned tailings dams and three seismic Intensity Measures (IM) in the free field: (a) Arias Intensity *AI*, (b) peak ground acceleration *PGA*, and (c) peak ground velocity *PGV* for the169 dynamic simulations.

correlations between the permanent vertical displacement *Uy* and the Arias Intensity, *AI* [35]; Fig. 7a), the Peak Ground Acceleration, *PGA* (Fig. 7b), and the Peak Ground Velocity, *PGV* (Fig. 7c). A linear regression of the natural logarithm of *Uy* and each IM was performed to evaluate the standard deviation of the regression error, $\sigma_{\ln(Uy)|IM}$, calculated as the Root Mean Square Error (RMSE) of the regression. The lower the $\sigma_{\ln(Uy)|IM}$, the higher the efficiency of the IM in predicting *Uy*.

Fig. 7 shows that the *AI* has the highest efficiency ($\sigma_{\ln(Uy)|IM} = 0.26$), which is consistent with the findings of [24] for slopes with a fundamental vibration period of 0.3 s, based on the analysis of a nonlinear fully-coupled stick-slip sliding block.

The efficiency of the 5%-damped spectral acceleration at different periods *Sa(T)* is quantified through the dispersion $\sigma_{\ln(Uy)|Sa(T)}$ in Fig. 8a. In the figure, the dispersion decreases for periods close to the fundamental vibration period of the slope, $T_0 = 0.3$ s, and remains relatively constant up to 0.5 s, which corresponds to 1.67 times the fundamental

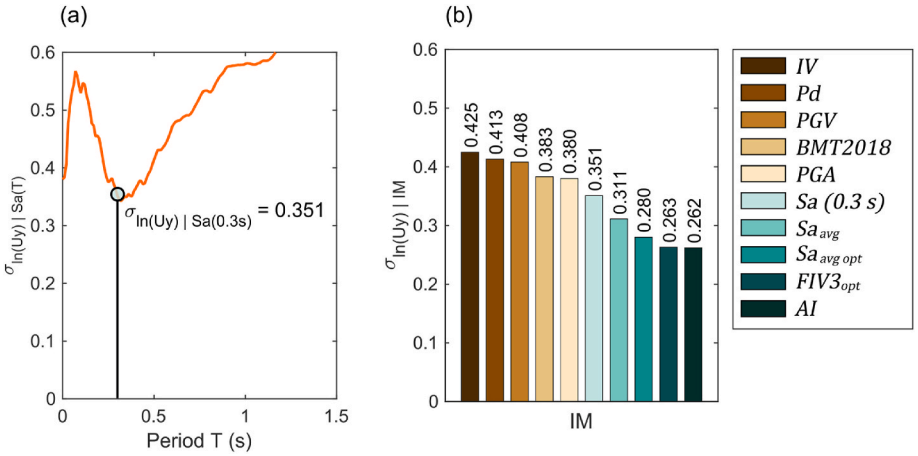

Fig. 8. (a) Dispersion of the permanent vertical displacement U_y conditioned to spectral accelerations with 5% damping ratio at different periods Sa(T). (b) Summary of dispersion indices for different IMs.

period. This range of high efficiency (i.e., low dispersion $\sigma_{\ln(Uy)|Sa(T)}$) may be associated with the resonance of the slope and stiffness degradation that occurs in the finite-element model.

Fig. 8b summarizes the efficiencies of the ten tested IMs: Incremental Velocity (IV [36]), Destructiveness Potential (P_d [37]), Peak Ground Velocity (*PGV*), permanent displacement estimated with the [34] method (*BMT2018*), Peak Ground Acceleration (*PGA*), Spectral Acceleration at 0.3 s [*Sa(0.3 s)*], Average Spectral Acceleration (Sa_{avg}, average of 10 values of spectral acceleration equispaced between 0.2 and 3 times the fundamental period of structure [38]), Optimized Average Spectral Acceleration ($Sa_{avg\ opt}$, average of 10 values of spectral acceleration equispaced between 0.6 and 1.8 times the fundamental period of structure), Optimized Filtered Incremental Velocity at 0.3 s [$FIV3_{opt}$ (f_c = 6.67 Hz, α = 0.2), [39]], and Arias Intensity (*AI*, [35]). We computed the parameters for the optimized IMs $FIV3_{opt}$ and $Sa_{avg\ opt}$ by minimizing the dispersion $\sigma_{ln(Uy)|IM}$. Fig. 8b indicates that *AI* and $FIV3_{opt}$ are the most efficient IMs for estimating *Uy* in this model. $Sa_{avg\ opt}$, Sa_{avg} and *Sa(0.3 s)* are also efficient alternatives.

The total uncertainty in a probabilistic seismic demand analysis does not depend only on the efficiency of the IM, but also on its predictability. In this context, *PGA* and spectral accelerations at different periods of vibration *Sa(T)* can be estimated within the Chilean subduction zone with the ground motion models (GMM) developed by Refs. [40,41]. These GMMs have logarithmic standard deviations between 0.64 and 0.91 in the period range between 0 and 10s. On the other hand, the Arias Intensity *AI* can be estimated with the GMM developed by Ref. [42], which has a logarithmic standard deviation of 1.19. In summary, although *AI* has higher efficiency than the spectral acceleration at a period of 0.3 s (see Fig. 8b), it also has a much lower predictability. Finally, *PGV* can be estimated using the model recently developed by Ref. [43] for the Chilean subduction zone, but the efficiency of PGV is lower than the other analyzed alternatives (see Fig. 8b). Considering that the rest of the considered IMs lack a GMM calibrated for the Chilean territory, the 5%-damped spectral acceleration at 0.3 s [*Sa (0.3 s)*] is chosen as the IM for the subsequent Multiple Stripe Analysis.

4.1. Ground motion record selection

We selected a set of 30 ground motion records to perform a Multiple-Stripe Analysis [44] at five different intensity levels. The database of ground motions consisted of 169 pairs of horizontal records of interface earthquakes with magnitudes larger than Mw 7.7 in Chilean territory, and the selected set was chosen by using the Conditional Spectrum, CS [45,46]. The conditioning period of the CS T^* was the fundamental period of the slope:T^* = 0.3 s. We calculated the target spectrum with the [40] GMM, evaluated for a characteristic interface earthquake magnitude Mw 8.0, rupture distance of 50 km, average shear-wave velocity in the top 30 m V_{s30} = 800 m/s, and soil type I (i.e., H/V spectral amplitude lower than 2 in the entire period range). We also used the interperiod correlation model for spectral accelerations developed by Ref. [47]. We set the parameter $\varepsilon(T^*) = 1$ to select the set of ground motion records. This choice limits the scale factor applied to the selected ground motions to less than 4 when scaled to the largest intensity level, as recommended by Ref. [48], in order to avoid a significant bias in the seismic response.

The selection of the ground motion records that match the target CS was performed with the optimization algorithm developed by Refs. [49,50]. Seismic stations installed over stiff soils and rock were preferred due to the characteristics of the foundation soils of the abandoned tailings dams. The spectra of 30 selected ground motions are shown in Fig. 9. The median and the dispersion (shown by the 2.5 and 97.5th percentiles) of the set of ground motion records closely match the target CS.

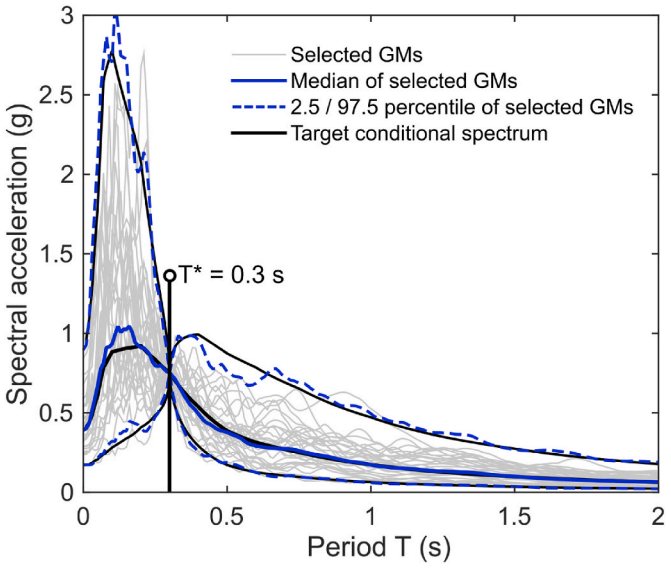

Fig. 9. Thirty selected ground motion records and their match to the target Conditional Spectrum.

5. Development of fragility curves

The fragility curves developed in this article present the probability of exceeding a given damage state, conditioned on a ground shaking intensity level, *P(DS|IM)*. These curves can be obtained through Equation (1), which is an application of the Total Probability Theorem.

$$P(DS|IM) = \int P(DS|EDP) \cdot f_{EDP}(edp|IM) \cdot d(edp) \tag{1}$$

where *P(DS|EDP)* is the probability of a given damage state conditioned on a value of *EDP*, and $f_{EDP}(edp|IM)$ is the probability density function of the EDP conditioned on a ground motion intensity.

The seismic response of the tailings dam, characterized by $f_{EDP}(edp|IM)$, is obtained through a Multiple Stripe Analysis (MSA, [44]). For this study, five ground shaking intensity levels were considered, *Sa (0.3s)* = 0.3, 0.6, 0.9, 1.2 and 1.5 g.

Due to the large variability of the cohesion parameter, *c,* in this type of structures, we developed three models with different cohesions to study the sensitivity of the results: the base level c = 7 kPa, a lower level c = 4.76 kPa, and an upper level c = 10.29 kPa. These lower and upper values represent the 16th and 84th percentiles of *c*, considering a lognormal distribution with a median of 7 kPa and a lognormal standard deviation of 0.4 [16].

Results of the MSA are shown in Fig. 10, where each point represents the permanent vertical displacement *Uy* of a numerical simulation performed with one of the ground motion records scaled to a given spectral acceleration *Sa(0.3s)*. The mean and the dispersion of *Uy* increase with increasing the ground shaking intensity. These trends exacerbate as the cohesion decreases due to lower shear strength.

The distribution of *Uy* at each stripe is parameterized through a lognormal distribution, as follows:

$$f_{Uy}(x \mid Sa\left(0.3\ s\right), c) = \frac{1}{x\,\beta\,\sqrt{2\pi}} \cdot \exp\left(-\frac{1}{2} \cdot \left(\frac{\ln(x) - \ln(\widehat{Uy})}{\beta}\right)^2\right) \tag{2}$$

where $\widehat{Uy}$ is the median of *Uy*, and β is its logarithmic standard deviation. These values are shown in Table 3.

The probability of reaching a damage state conditioned on a value of EDP, *P(DS|EDP)* in Equation (1) can be determined by analyzing the serviceability state of the analyzed structure. For the case of abandoned tailings dams, performance states associated to serviciability levels have

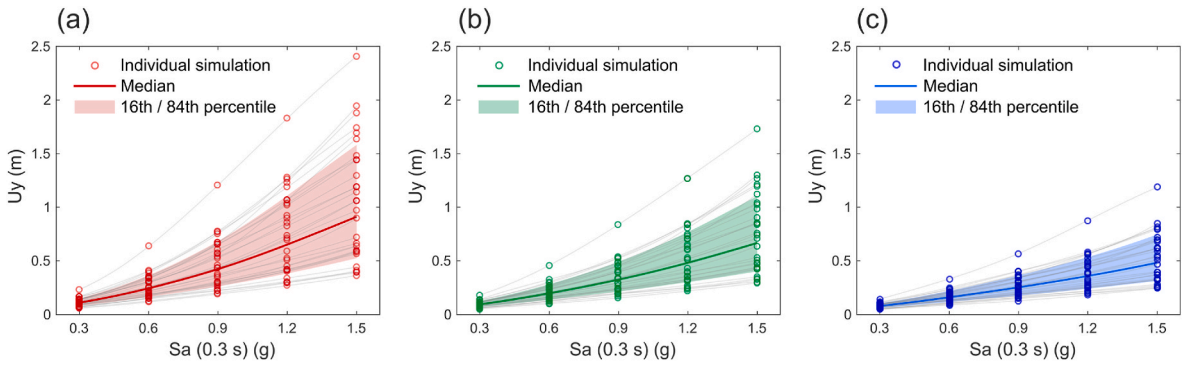

Fig. 10. Multiple Stripe Analysis performed with nonlinear dynamic simulations of models with (a) $c = 4.76$ kPa, (b) $c = 7.00$ kPa, and (c) $c = 10.29$ kPa.

Table 3
Parameters of lognormal distributions of *Uy* as a function of *Sa(0.3s)* and *c*, obtained from the Multiple Stripe Analysis.

Cohesion, c (kPa)	*Sa(0.3s) (g)*	Median, $\widehat{Uy}$ (m)	Log. standard deviation, β
4.76	0.3	0.111	0.326
	0.6	0.245	0.404
	0.9	0.423	0.478
	1.2	0.651	0.533
	1.5	0.910	0.553
7.00	0.3	0.095	0.296
	0.6	0.198	0.356
	0.9	0.325	0.411
	1.2	0.481	0.468
	1.5	0.666	0.505
10.29	0.3	0.080	0.279
	0.6	0.161	0.317
	0.9	0.254	0.361
	1.2	0.359	0.398
	1.5	0.483	0.434

not been defined, except for an extreme collapse state. For this reason, we propose to evaluate the structural integrity and physical stability of the tailings dam by analyzing the final stress field of the numerical model.

The permanent vertical displacement, *Uy*, used to evaluate the seismic response of the dam is a consequence of plastic strains at multiple integration points of the finite-element model. These points have a shear strength, given by the Morh-Coulomb failure criterion adopted in the HSS model. The number of points in this ultimate stress state reflects the incursion of the dam into large displacements and highlights the slope zones unable to sustain larger shear stresses. Fig. 11a shows with red dots the integration points that reached their shear strength when the dam model is subjected to the ground motion described in Section 3 and shown in Fig. 5a. Displacement localization indicated by the shear strains contours concentrates around the pseudo-static limit-equilibrium method (LEM) critical failure surface.

The failure area ratio, *FAR*, is introduced to account for numerical model plastification, and it is defined as follows:

$$FAR = \left(\sum A_f\right) \Big/ A_t \tag{3}$$

where A_f is the equivalent area of integration points reaching the ultimate shear strength, calculated as the total area of the corresponding finite element divided by the number of integration points (i.e., 12), and A_t is the total area of interest, as shown in Fig. 11b. Some elements inside A_t are unlikely to reach a plastic state. However, we just considered A_t as normalization area, understanding that *FAR* cannot necessarily range from 0 to 1.

Fig. 12 shows the permanent vertical displacement, *Uy*, as a function of failure area ratio *FAR* of the 450 dynamic analyses (i.e., 3 models • 5 stripes • 30 ground motions per stripe). The clear relationship between *Uy* and *FAR* is used to estimate the model damage states. The trend of the point cloud is fitted with the following rational function:

$$FAR(Uy) = \frac{\sum_{i=1}^{n+1} p_i \bullet (Uy)^{n+1-i}}{Uy^m + \sum_{i=1}^{m} q_i \cdot Uy^{m-1}} \tag{4}$$

where n and m are constants (n = m = 5) and the values of the model coefficients p_i and q_i are shown in Table 4. The regression is characterized by a $R^2 = 0.97$ and RMSE = 0.035.

Three zones characterize the relationship between *Uy* and *FAR* (Fig. 12a): (1) *FAR* is almost negligible for $Uy < 0.25$ m, (2) *FAR* increases at a high rate for $0.25\text{ m} < Uy < 0.6$ m, and (3) FAR increases at a lower rate for $Uy > 0.6$ m. These three zones are used to define three damage levels: slight, moderate, and severe damage, respectively.

These damage states are consistent with the contours of shear strains

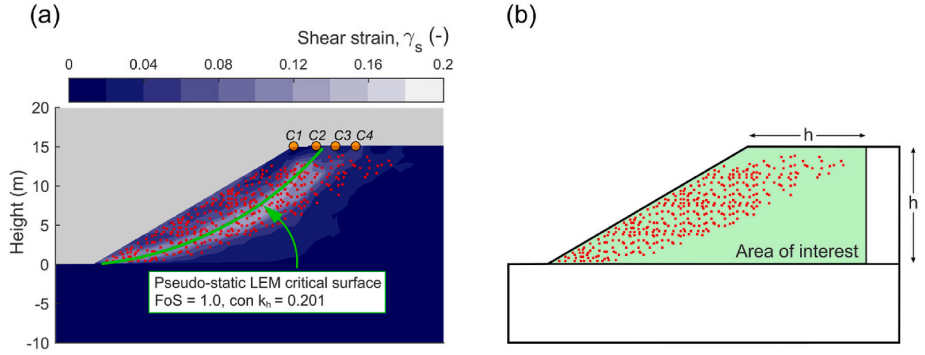

Fig. 11. (a) Contour of residual shear strains after dynamic loading, highlighting the integration points that reached their ultimate shear strength (red dots) and the critical surface from a pseudo-static LEM analysis. (b) Definition of the area of interest (A_t in Equation (3)).

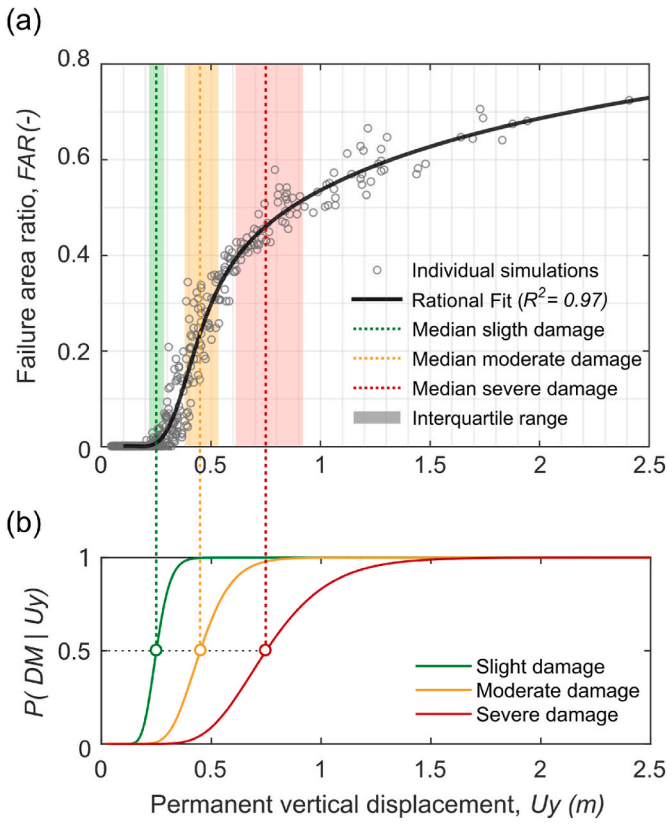

Fig. 12. (a) Relationship between failure area ratio *FAR* and permanent vertical displacement *Uy*. (b) Parameterization of the probability of reaching a damage state DM given *Uy*, *P(DM|Uy)*.

Table 4
Coefficients for the rational function fitting the relationship between *Uy* and *FAR* (see Equation (4)).

Coefficient	Value (–)	Coefficient	Value (–)
p_1	1.209	q_1	5.137
p_2	2.636	q_2	0.846
p_3	1.433	q_3	3.098
p_4	−1.104	q_4	−2.746
p_5	0.185	q_5	0.777
p_6	−0.008	–	–

and failure points in the executed models:

- Slight damage corresponds to the beginning of slope failure and slight increase in *FAR*.
- Moderate damage corresponds to a high rate of *FAR* development and the beginning of the concentration of plastic deformations in the vicinity of the pseudo-static LEM critical surface.
- Severe damage is characterized by a lower rate of *FAR* development, strong stress concentration, and pronounced strain localization around the pseudo-static LEM critical surface. The rate of *FAR* development decreases due to stress redistribution. In this stage, extensive slope areas reach their ultimate shear strength, which compromises the global physical stability.

The three levels of damage are parameterized with a lognormal cumulative function (Equation (5)), which characterizes the transition between the zones defined by the rational fit (see Fig. 12a) and represents the probability of reaching or exceeding a specific damage state DS conditioned on a value of permanent vertical displacement, *Uy*:

$$P(DS|Uy) = \Phi\left(\frac{\ln(Uy/\theta)}{\beta}\right) \quad (5)$$

where Φ is the standard normal cumulative density function, θ is the function median, and β is the logarithmic standard deviation. These functions are defined with the coefficients in Table 5 and depicted in Fig. 12b.

Once the probability density function of *Uy* and the cumulative distribution functions of the different damage states are obtained, Equation (1) is evaluated. The evaluation of Equation (1) results in a scalar that indicates the probability of reaching or exceeding a certain damage state for a given ground shaking intensity (squares in Fig. 13). From these results, fragility curves can be obtained from a parametric fit using various procedures [51]. In this study, we performed a least-squares regression adjustment.

The curves in Fig. 13 are complemented with a 95% confidence interval, obtained using a Bootstrap method [52], consisting of resampling with replacement the set of 30 base seismic records and repeating the entire fragility curve fitting procedure 20,000 times. Therefore, the intervals' limits correspond to the 2.5 and 97.5 percentiles of the empirical fragility curves obtained for the 20,000 bootstrap samples. Fig. 13 shows three sets of fragility curves for the models with different cohesions. We argue, in the next section, that these curves could represent the seismic vulnerability of slope models characterized by their horizontal yield seismic coefficient k_y.

6. Sensitivity analysis

The horizontal yield seismic coefficient, k_y, has been used to characterize the seismic slope stability by numerous studies on seismic displacements [24,33,34,53]. In this section, we study the feasibility of using this parameter to select the proper set of fragility curves shown in Fig. 13 through a sensitivity analysis. As Fig. 6 shows for the base case, the yield seismic coefficient, under which the factor of safety is lower than unity, is $k_y = 0.201$.

The sensitivity analysis consists of simulating the seismic response of models that differ from the cases analyzed in the previous section in just one parameter. The parameters modified in this section are:

- **Slope angle**: Two models with slope angles of 33.34° and 25.61° were developed. For both models, the cohesion, the internal friction angle, and the dam height were set at 7 kPa, 30°, and 15 m. The horizontal yield seismic coefficients of these models are $k_y = 0.156$ and $k_y = 0.260$, respectively.
- **Internal friction angle:** Two models with internal friction angles of 33.15° and 27.55° were developed. For both models, the cohesion, the slope angle, and the dam height were set at 7 kPa, 30°, and 15 m. The horizontal yield seismic coefficients of these models are $k_y = 0.260$ and $k_y = 0.156$, respectively.
- **Dam height:** Two models with dam height of 10 m and 20 m were developed. For both models, the cohesion, the slope angle, and the internal friction angle were set at 7 kPa, 30°, and 30°. The horizontal yield seismic coefficients of these models are $k_y = 0.260$ and $k_y = 0.156$, respectively.
- **Material stiffness:** Two models with stiffness parameters reduced by half and amplificated by 2 were developed. For both models, the

Table 5
Coefficients for the parameterization of Equation (5), which define the three damage states.

Damage level	Median, θ	Log. standard deviation, β
Slight damage	0.25	0.20
Moderate damage	0.45	0.25
Severe damage	0.75	0.30

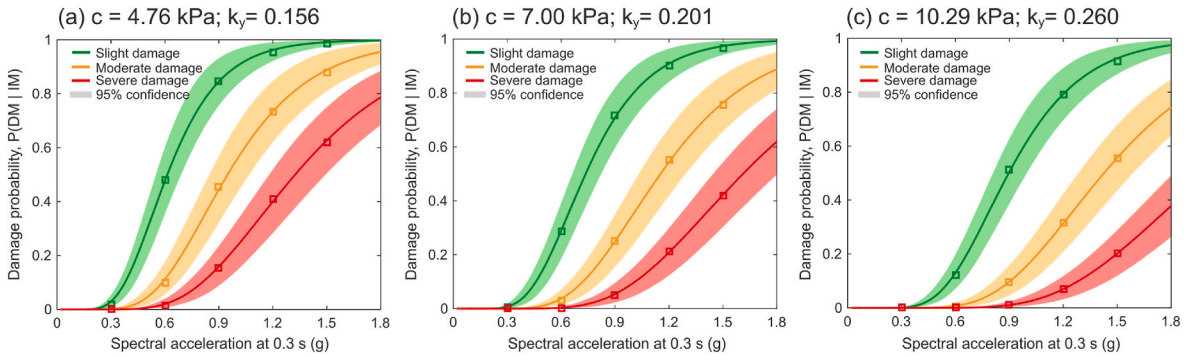

Fig. 13. Fragility curves for abandoned tailings dams with different cohesions (a) c = 4.76 kPa, (b) c = 7 kPa, and (c) c = 10.29 kPa. The shaded areas around the mean curves are the confidence intervals obtained using Bootstrapping.

cohesion, the slope angle, the internal friction angle, and the dam height were set at 7 kPa, 30°, 30°, and 15 m. As the limit equilibrium method assumes the materials are rigid perfectly-plastic, the material stiffness does not influence the factor of safety estimated with this method. Then, the horizontal yield seismic coefficient of these models remains at $k_y = 0.201$. The stiffness is adjusted in the models by changing the four moduli of the tailings material (E_{50}^{ref}, E_{oed}^{ref}, G_0^{ref}, E_{ur}^{ref}).

These models were subjected to three ground motions scaled at intensity levels *Sa(0.3s)* = 0.3, 0.6, 0.9, 1.2, and 1.5 g. These three seismic records were selected to have three different spectral shapes in order to account for the role of the input motion characteristics from the modified models. The sensitivity analysis aims at comparing the damage in the additional models and that in the models shown in the previous section that have the same horizontal yield seismic coefficients.

The permanent vertical displacement, *Uy*, is the result of strain integration of multiple finite elements in the tailings dam model. Therefore, when the *Uy* of a low-height slope is similar to that of a taller slope, the elements of the former model have experienced larger strains. This effect is captured in several studies that estimate dam damage by a normalized settlement with respect to the total dam height (e.g., Refs. [27,28].

The material damage is estimated in this study from the integration points that reach their ultimate shear strength in the finite element model. If two materials have the same strength, the more ductile one has a larger deformation tolerance before reaching the shear strength. Hence, the estimated damage depends on the material stiffness.

The normalized displacement Uy_n, defined as follows, is proposed to consider the combined effect of dam height and material stiffness:

$$Uy_n = \frac{Uy}{h \cdot \varepsilon_f} \tag{6}$$

where h is the dam height and ε_f is a reference strain at which a numerical triaxial test confined at the average stress of the elements in the area of interest, defined in Fig. 11b, reaches the shear strength.

The use of Uy_n allows comparing models with different properties. Fig. 14 shows the results obtained in the additional models simulated in this section. Fig. 14a shows the failure area ratio *FAR* as a function of *Uy* and the poor adjustment of the trend compared to the adjustment in Fig. 12a. In contrast, Fig. 14b illustrates that the rational fit of the simulated data improves when Uy_n is considered.

In order to compare the results of different dam models, the normalized error is defined as

$$\varepsilon_n^S = \frac{Uy_n^B - Uy_n^S}{Uy_n^B} \tag{7}$$

where Uy_n^B is the normalized displacement of the Base Case models characterized by k_y and Uy_n^S is the normalized displacement of the sensitivity model characterized by the same value of k_y.

Positive ε_n^S values mean that the base case model experiences a larger normalized displacement than the sensitivity model with the same k_y. Hence, the use of the proposed fragility curves in Fig. 13 for damage assessment of the sensitivity model would be conservative. Fig. 15 shows the normalized error for each sensitivity model, subjected to the 3 selected seismic records, and scaled to 5 intensity levels, so that each stripe contains 15 dots. The Figure shows that the normalized errors are less than 20% in all cases, indicating that k_y can represent the overall resistance of a slope.

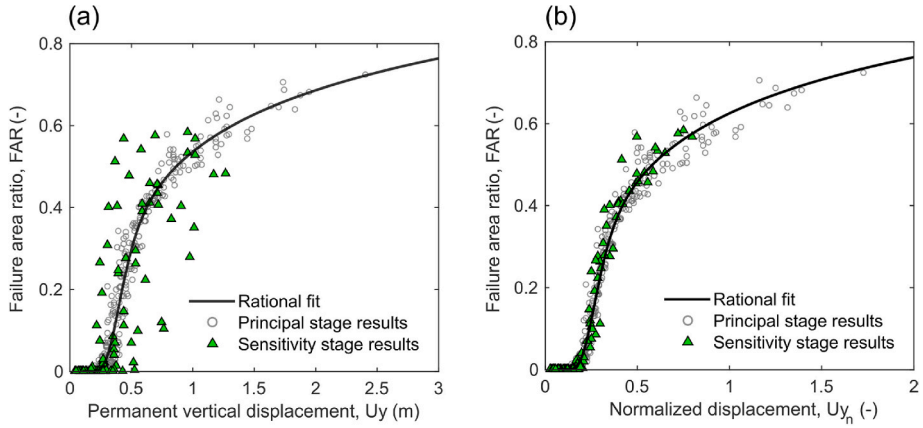

Fig. 14. Failure area ratio *FAR* as a function of (a) permanent vertical displacement, *Uy* and (b) normalized displacement Uy_n.

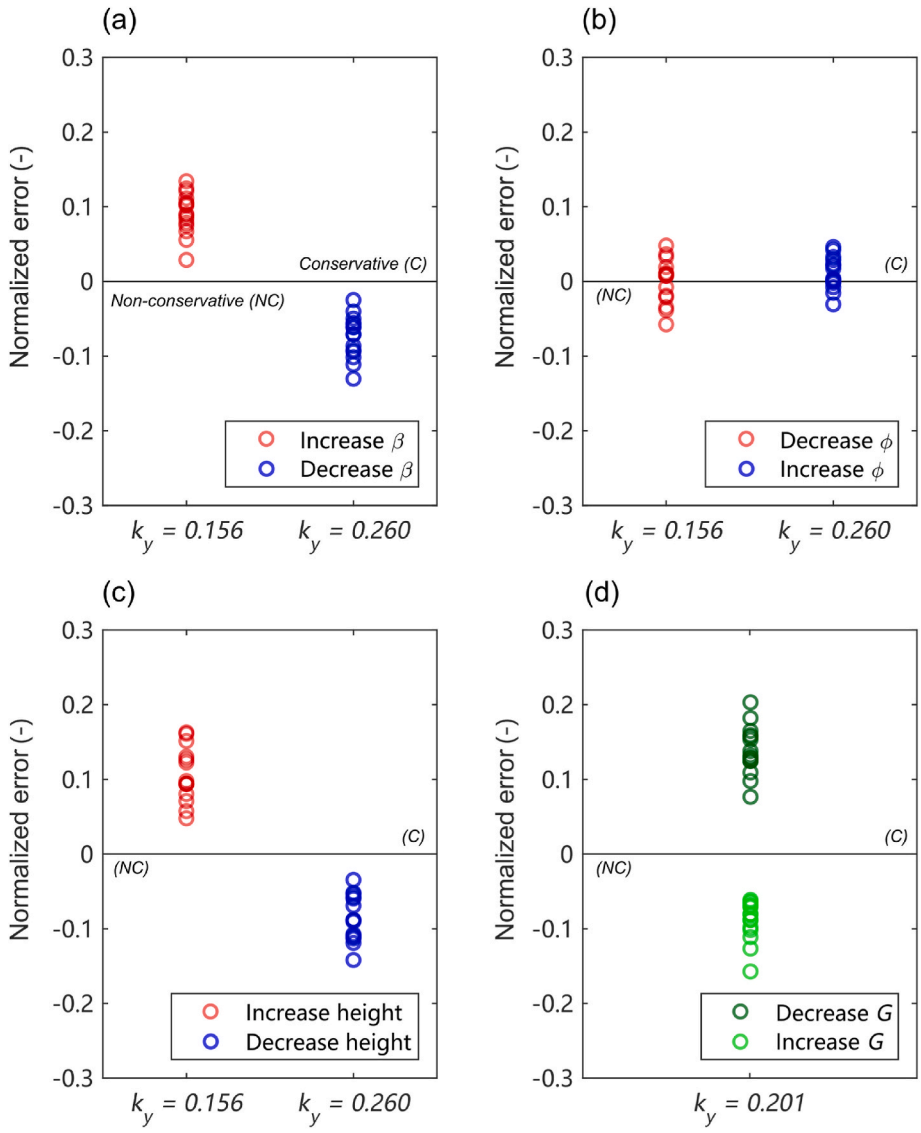

Fig. 15. Results of sensitivity analysis for (a) slope angle β (b) tailings friction angle φ, (c) dam height h, (d) tailings stiffness.

7. Discussion

The validation of the proposed fragility curves is a complex task due to the lack of geotechnical surveys that allow calculating the seismic yield coefficient. Nonetheless, it is possible to perform some verification exercises.

The first validation exercise is the case of the city of Andacollo, where the seismic station C10O is installed and 13 abandoned tailings dams are located within 1-km radius around this station. These structures were affected by the 2015 Mw 8.3 Illapel Earthquake, whose rupture area is estimated to be approximately 90 km away from Andacollo (see Fig. 1; [54]). The recorded spectral acceleration for a vibration period of 0.3 s at the station C10O was Sa(0.3 s) = 0.33 g. Evaluating this spectral acceleration in all the fragility curves in Fig. 13 results in a negligible probability of severe damage, even considering the 95% confidence interval. The 13 abandoned tailings dams performed well during this earthquake, with no damage being recorded or estimated from visual inspection and satellite images, keeping consistency with the proposed fragility model.

A similar exercise can be performed with the abandoned tailings dams failures reported in Ref. [2], classified as slope instability with seismically induced deformations. Table 6 presents the details of this validation exercise, where Sa(0.3 s) was estimated from the records of the nearest seismic station and the maximum probability of severe damage is the highest confidence limit of severe damage given by the curve for c = 4.76 kPa, that is, the worst-case scenario. In all these cases, the fragility curve in Fig. 13a predicts a certain probability that the tailing dam would show severe damage. Failures due to liquefaction reported in Ref. [2] were not considered since our study does not consider this phenomenon.

Although liquefaction is an important trigger mechanism of tailings dams failures, Villavicencio et al. [2] determined that nearly 60% of earthquake failures of abandoned tailings dams in Chile are due to the mechanism slope instability with seismically induced deformations, in which there was no evidence of liquefaction. This mechanism is believed to manifest when the dams are in unsaturated conditions due to the long-term loss of water content favored by the arid weather where these dams are located. Nonetheless, it is important to estimate the degree of saturation and the saturation profile in abandoned tailings dams, which allows calculations of the potential development of cyclic mobility and flow liquefaction.

Table 6
Verification of fragility curves according to the seismic performance of abandoned tailings dams.

Tailings dam	Earthquake	Nearest Station (Distance)	Sa (0.3s) (g)	Response	Max. estimated probability of severe damage
Cobre No.4	Valparaíso 1985	Llay Llay (30 km)	1.12	Failure	44%
Tranque Planta Chacón	Maule 2010	Melipilla (60 km)	0.69	Failure	8%
Veta del Agua No.5	Maule 2010	Cabildo (30 km)	0.89	Failure	22%
Tranque No.1 Minera Clarita	Maule 2010	Cabildo (40 km)	0.89	Failure	22%
Andacollo dams (13)	Illapel 2015	Andacollo (<1 km)	0.33	No damage	0%

Note: Failure of abandoned tailings dams previous to 2015 are reported in Ref. [2] as "slope instability with seismically-induced deformations".

7.1. The Delirio A tailings dam

The exploration campaign of the Delirio A abandoned tailings dam determined that the parameters that represent the deposit are h = 21 m, φ = 25°, c = 17 kPa, and β = 36°. These parameters result in a critical yield coefficient of $k_y = 0.148$, a value slightly lower than $k_y = 0.156$ (fragility curves in Fig. 13a). The [40] GMM is used to estimate *Sa(0.3 s)* at the site of the tailings dam, due to the 2015 Illapel Earthquake, considering a moment magnitude $M_w = 8.3$, a closest distance to rupture area $R = 62$ km, $V_{s30} = 1200$ m/s, and soil type I. Then, we compute the probability of damage as follows:

$$P(DS) = \int P(DM|Sa) \cdot f_{sa}(sa) \cdot d(sa) \tag{8}$$

where *P(DS|Sa)* corresponds to the fragility curve for a given damage state, and $f_{sa}(sa)$ is the probability distribution of spectral accelerations at a vibration period of 0.3 s estimated by the GMM. Results indicate that the probability of presenting slight, moderate, and severe damage due to the 2015 Illapel Earthquake are 31%, 17%, and 3%, respectively.

Fig. 16 shows aerial images of the Delirio A tailings dam where longitudinal cracks are observed at the top of the wall, which could be attributed to seismic deformation and considered as a state of slight-to-moderate damage.

In order to complement this analysis, a 2D model of the Delirio A tailings dam was built, considering the parameters mentioned above (h = 21 m, φ = 25, c = 17 kPa, β = 36°). The other parameters of the HSS constitutive model were assumed as those shown in Table 2. The model was subjected to a ground motion record whose response spectrum minimizes the sum of the squared errors with respect to the target spectrum defined in Fig. 9, scaled to *Sa(0.3 s)* = 1.2g. We compared the results of this model with the base case model with the nearest k_y (k_y = 0.156) subjected to the same ground motion.

Fig. 17 compares the base case model $k_y = 0.156$ and the Delirio A model in terms of residual shear strain and failure points. Although the vertical displacement is $U_y = 0.7$ m in both cases, the base case model shows significantly more damage. The extend of the damage is captured by the normalized vertical displacement Uy_n, which is larger for the base case model ($Uy_n = 0.5$). Despite the differences in damage and the large variation of model parameters, the probability of attaining moderate-severe damage for both models is similar, as predicted by the fragility curve in Fig. 13. Then, the fragility curve can be applied for a variety of slope parameters if the yield coefficient of the slope is close to those considered in the principal stage of this study.

The use of the proposed fragility curves along with seismic hazard maps can support preliminary seismic vulnerability evaluation of a large portfolio of abandoned tailings dams while site-specific data is generated by the authorities. The results can inform decisions of investment in further geotechnical characterization or reinforcement of the most vulnerable dams.

8. Conclusions

This work proposes a set of fragility curves for estimating the probability of damage in abandoned tailings dams in North-Central Chile as a function of the spectral acceleration at a vibration period of 0.3s, *Sa (0.3s)*, and the seismic yield coefficient of the slope, k_y. The latter parameter seeks to characterize the variables involved in the slope stability of the resistant structure and can be obtained through a pseudo-static limit equilibrium analysis.

The ground-shaking intensity measure (IM) selected in this study, *Sa (0.3s)*, shows a lower efficiency than other evaluated intensities, such as *AI*, Sa_{avg}, $Sa_{avg,opt}$ and $FIV3_{opt}$. However, *Sa(0.3s)* was finally selected due to its high predictability when compared to the more efficient alternatives. For example, the Arias Intensity was the most efficient *IM* to predict seismic displacements in the proposed model at the intensity values evaluated, but the available GMM presents a significantly larger dispersion.

Damage states are estimated by interpreting the relationship between the failure area ratio *FAR* within the slope and the permanent vertical displacement of the crest. This trend can be reproduced for

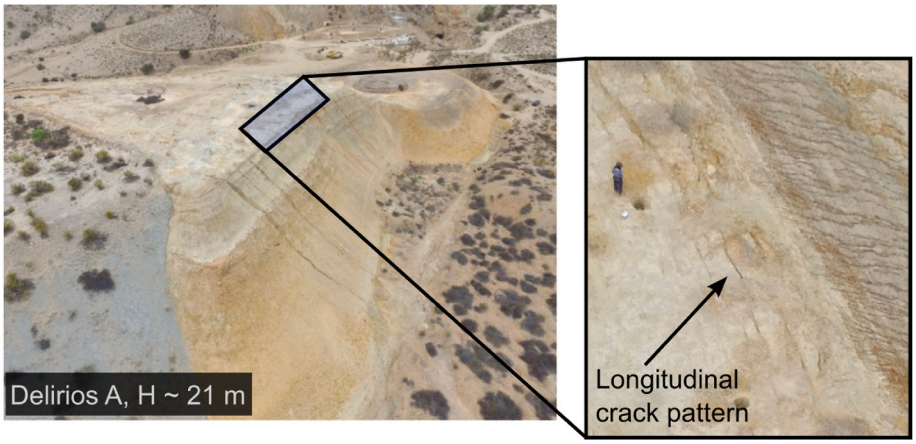

Fig. 16. Drone images of the Delirio A tailings dam, where the pattern of longitudinal cracks is observed along the crest of the southeast slope.

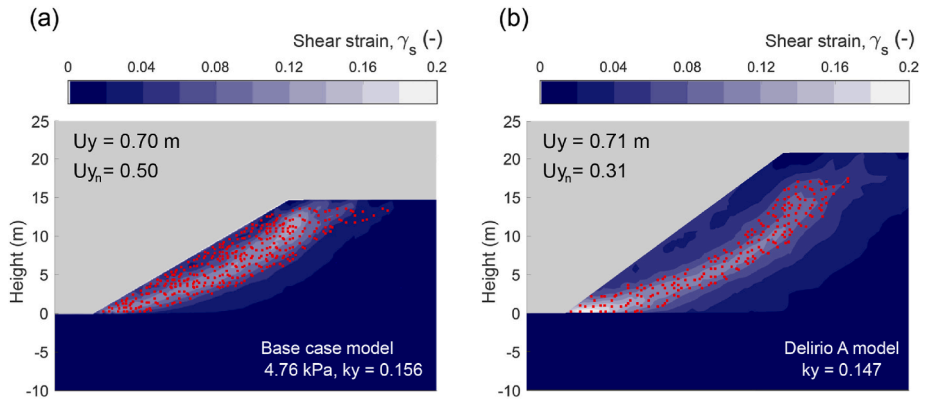

Fig. 17. Shear strain contour comparison of two dynamic models subjected to the same seismic record: (a) base case model with $k_y = 0.156$, (b) representative model of the Delirio A dam. Red dots are the integration points that reached their shear strength.

models with different properties by normalizing the permanent vertical displacement by the height of the slope and the principal axial failure strain of the material. Therefore, the proposed fragility curves can be extended to various slopes with different geometries and material properties.

The fragility curves are consistent with the reported historical Chilean tailings dam failures due to earthquake-induced deformation. Likewise, they are compatible with the seismic performance of the abandoned dams affected by the 2015 Mw 8.3 Illapel Earthquake, during which abandoned tailings dams did not present visible damage. In this context, it is essential to assess these fragility curves as additional information becomes available in future studies.

For a horizontal yield coefficient $k_y = 0.201$, the proposed fragility curves predict approximately 10% probability of severe damage for Sa (0.3s) = 1g, a spectral value that has been measured in 20 seismic stations of the Chilean strong-motion network in the last 12 years. For this reason, it is crucial to continue the evaluation of abandoned tailings dams and to carry out remediation actions in those that present unacceptable risk levels.

It should be emphasized that the proposed fragility curves are intended for a preliminary evaluation of the seismic vulnerability of abandoned tailings dams and a tool for detecting those dams requiring further studies and remediation measures. The scope is limited to small-size abandoned tailings dams (h < 25 m) in a region with semi-arid weather, which favors long-term loss of water, and subjected to interface earthquakes. The model must be carefully applied, since several assumptions must be verified, such as the slope height, the material homogeneity, a low degree of saturation, and the absence of water table, among others.

Credit author statement

Gonzalo Boada: Methodology, Formal analysis, Investigation, Visualization, Writing - Original Draft. César Pastén: Funding acquisition, Project administration, Supervision, Conceptualization, Writing - Review & Editing. Pablo Heresi: Conceptualization, Writing - Review & Editing.

Declaration of competing interest

The authors declare that they have no known competing financial interests or personal relationships that could have appeared to influence the work reported in this paper.

Data availability

Data will be made available on request.

Acknowledgements

Support for this research was provided by the Advanced Mining Technology Center (AMTC PIA ANID grant AFB180004). César Pastén thanks the support from the ANID Fondecyt grant N°1190995.

References

[1] Verdugo R, Sitar N, Frost DJ, Bray JD, Candia G, Eldridge T, Hashash Y, Olson SM, Urzúa A. Seismic performance of earth structures during the February 2010 Maule, Chile, earthquake: dams, levees, tailings dams, and retaining walls. Earthquake Spectra EERI 2012;28(S1):S75–96.
[2] Villavicencio G, Espinace R, Palma J, Fourie A, Valenzuela P. Failures of sand tailings dams in a highly seismic country. Can Geotech J 2013;51(4):449–64.
[3] Sernageomin. Catastro de Depósitos de Relaves en Chile (updated 10-08-2020) [online]. www.sernageomin.cl. [Accessed 20 September 2021]. Accessed on.
[4] Chile Fundación, Tranque Programa. Avances y retos para la gestión de los depósitos de relaves en Chile [online]. www.fch.cl. [Accessed 20 September 2021] [Accesed on.
[5] Krawinkler H, Miranda E. Performance-based earthquake engineering. In: Bozorgnia Y, Bertero VV, editors. Earthquake engineering: from engineering seismology to performance-based engineering. Boca Raton: CRC Press; 2004.
[6] Argyroudis S, Kaynia A. Analytical seismic fragility functions for highway and railway embankments and cuts. Earthq Eng Struct Dynam 2015;44:1863–79.
[7] Oblak A, Kuder S, Logar J, Da Fonseca AV. Numerical assessment of fragility curves for embankments on liquefiable ground. In: Proceedings of the XVII ECSMGE-2019, reykyavik, Iceland, 1–7 september; 2019.
[8] Argyroudis S, Kaynia AM, Pitilakis K. Development of fragility functions for geotechnical constructions: application to cantilever retaining walls. Soil Dynam Earthq Eng 2013;50:106–16. 2013.
[9] Ruiz S, Madariaga R. Historical and recent large megathrust earthquakes in Chile. Tectonophysics 2018;733:37–56.
[10] Fernández J, Pastén C, Ruiz S, Leyton F. Damage assessment of the 2015 Mw 8.3 Illapel earthquake in the North-Central Chile. Nat Hazards 2018;96:269–83.
[11] Pulgar B. Methodology to evaluate the physical stability of abandoned tailings dams in North-Central Chile. Civil Engineer Dissertation. Santiago, Chile: University of Chile, Department of Civil Engineering; 2020.
[12] Nakamura Y. A method for dynamic characteristics estimation of subsurface using microtremor on the ground surface. QR Railway Technical Research Institute 1989; 30(1):25–33.
[13] Borcherdt RD. Effects of local Geology on ground motion near san francisco rbay. Bull Seismol Soc Am 1970;60:29–61.
[14] Wathelet M, Chatelain J, Cornou C, Di Giulio G, Guillier B, Ohrnberger M, Savvaidis A. Geopsy: a user-friendly open-source tool set for ambient vibration processing. Seismol Res Lett 2020;91(3):1878–89.
[15] Pastén C, Sáez M, Ruiz S, Leyton F, Salomon J, Poli P. Deep characterization of the Santiago Basin using HVSR and cross-correlation of ambient seismic noise. Eng Geol 2016;201:57–66.
[16] Duncan J. Factors of safety and reliability in geotechnical engineering. Journal of Geotechnical and Geoenvironmental Engineering ASCE 2000;126(4):307–16.
[17] Vick SG. Planning, design, and analysis of tailings dams. Vancouver, B.C. Canada: BiTech Publishers Ltd; 1990.
[18] Plaxis. PLAXIS 2D reference manual. Dublin: Bentley Systems International Limited; 2019.
[19] Hashash Y, Musgrove M, Harmon J, Ilhan O, Xing G, Numanoglu O, Groholski D, Phillips C, Park D. DEEPSOIL 7.0, user manual. Urbana, IL: Board of Trustees of University of Illinois at Urbana-Champaign; 2020.
[20] Tsai C, Park D, Chen C. Selection of the optimal frequencies of viscous damping formulation in nonlinear time-domain site response analysis. Soil Dynam Earthq Eng 2014;67:353–8.

[21] Darendeli M. Development of a new family of normalized modulus reduction curves and material damping curves. PhD thesis. The University of Texas at Austin; 2001.
[22] Ishibashi I, Zhang X. Unified dynamic shear moduli and damping ratios of sand and clay. Soils Found 1993;33:182–91.
[23] Kuhlemeyer R, Lysmer J. Finite element method accuracy for wave propagation problems. J Soil Mech Found Div 1973;99:65.
[24] Bray J, Travasarou T. Simplified procedure for estimating earthquake-induced deviatoric slope displacements. J Geotech Geoenviron Eng 2007;133(4):381–92.
[25] GEO-SLOPE International Ltd. Stability modeling with SLOPE/W, an engineering methodology. July 2012. Edition 2012. Calgary, Alberta, Canada.
[26] Morgenstern NR, Price VE. The analysis stability of general slip surfaces. Geotechnique 1965;15(1):79–93.
[27] Pells S, Fell R. Damage and cracking of embankment dams by earthquake and the implications for internal erosion and piping. Montréal, Canada: Commission International Des Grands Barrages; 2003.
[28] Swaisgood J. Predicting dam deformation caused by earthquakes - an update, vol. 2. Association of State Dam Safety Officials Annual Conference 2013; 2013. p. 970–80. Dam Safety 2013.
[29] Shome N, Cornell CA. Normalization and scaling accelerograms for nonlinear structural analysis. In: Proceeding., 6th US national conference on earthquake engineering. Oakland, CA: Earthquake Engineering Research Institute; 1998.
[30] Luco N, Cornell CA. Structure-specific scalar intensity measures for near-source and ordinary earthquake ground motions. Earthq Spectra 2007;23(2):357–92.
[31] Kramer SL, Mitchell RA. Ground motion intensity measures for liquefaction hazard evaluation. Earthq Spectra 2006;22(2):413–38.
[32] Poulos A, Monsalve M, Zamora N, de la Llera J. An updated recurrence model for Chilean subduction seismicity and statistical validation of its Poisson nature. Bull Seismol Soc Am 2019;109(1):66–74.
[33] Makdisi F, Seed H. Simplified procedure for estimating dam and embankment earthquake-induced deformations. J Geotech Eng Div 1978;104(7):849–67.
[34] Bray J, Macedo J, Travasarou T. Simplifed procedure for estimating seismic slope displacements for subduction zone earthquakes. Journal of Geotechnical and Geoenvironmental Engineering ASCE 2018;144(3):04017124.
[35] Arias A. A measure of earthquake intensity. In: Hansen R, editor. Seismic design for nuclear power plants. Cambridge: MIT Press; 1970. p. 438–83.
[36] Bertero V, Mahin S, Herrera R. Aseismic design implications of near-fault San Fernando earthquake records. Earthq Eng Struct Dynam 1978;6(1):31–42.
[37] Araya R, Saragoni GR. Earthquake accelerogram destructiveness potential factor. San Francisco, CA. In: Proc. 8th world conference on earthquake engng, EERI; 1985. p. 835–42. 1985.
[38] Eads L, Miranda E, Lignos DG. Average spectral acceleration as an intensity measure for collapse risk assessment. Earthq Eng Struct Dynam 2015;44:2057–73.
[39] Dávalos H, Miranda E. Filtered incremental velocity: a novel approach in intensity measures for seismic collapse estimation. Earthq Eng Struct Dynam 2019;48:1384–405.
[40] Idini B, Rojas F, Ruiz S, Pastén C. Ground motion prediction equations for the Chilean subduction zone. Bull Earthq Eng 2017;15(5):1853–80.
[41] Montalva G, Bastías N, Rodriguez-Marek A. Ground-motion prediction equation for the Chilean subduction zone. Bull Seismol Soc Am 2017;107(2):901–11.
[42] Céspedes S, Boroschek R, Ruiz R. Modelos de movimiento fuerte para duración e Intensidad de Arias para registros de movimiento fuerte en Chile. In: Conference: XII Congeso Chileno de Sismología e Ingeniería Antisísmica; 2019. Valdivia.
[43] Montalva G, Bastías N, Leyton F. Strong ground motion prediction model for PGV and spectral velocity for the Chilean subduction zone. Bull Seismol Soc Am 2022;112(1):348–60. Bulletin of the Seismological Society of America.
[44] Jalayer F. Direct probabilistic seismic analysis: implementing non-linear dynamic assessments. Ph.D. Thesis. Stanford, CA: Dept. of Civil and Environmental Engineering, Stanford University; 2003.
[45] Baker J, Cornell C. Spectral shape, epsilon and record selection. Earthq Eng Struct Dynam 2006;35(9):1077–95.
[46] Baker J. Conditional mean spectrum: tool for ground motion selection. J Struct Eng 2011;137(3):322–31.
[47] Candia G, Poulos A, de la Llera J, Crempien J, Macedo J. Correlations of spectral accelerations in the Chilean subduction zone. Earthq Spectra 2020;36(2):788–805.
[48] Dávalos H, Miranda E. Evaluation of bias on the probability of collapse from amplitude scaling using spectral-shape-matched records. Earthq Eng Struct Dynam 2019;48:970–86.
[49] Jayaram N, Lin T, Baker J. A computationally efficient ground-motion selection algorithm for matching a target response spectrum mean and variance. Earthq Spectra 2011;27:797–815.
[50] Baker J, Lee C. An improved algorithm for selecting ground motions to match a conditional spectrum. J Earthq Eng 2018;22(4):708–23.
[51] Baker J. Efficient analytical fragility function fitting using dynamic structural analysis. Earthq Spectra 2013;31(1):579–99.
[52] Efron B. Bootstrap methods: another look at the jackknife. Ann Stat 1979;7:1–26.
[53] Newmark N. Effects of earthquakes on dams and embankments. Geotechnique 1965;15(2):139–60.
[54] Ruiz S, Klein E, del Campo F, Rivera E, Poli P, Metois M, Vigny C, Baez JC, Vargas G, Leyton F, Madariaga R, Fleitout L. The seismic sequence of the 16 september 2015 Mw 8.3 Illapel, Chile, earthquake. Seismol Res Lett 2016;87.